physica status solidi

pss

www.pss-journals.com

reprint

WILEY-VCH

Phys. Status Solidi RRL **10**, No. 2, 164–167 (2016) / **DOI** 10.1002/pssr.201510367

High transmission nanowire contact arrays with subwavelength spacing

Etor San Román[1], Alan Vitrey[1], Jerónimo Buencuerpo[1], Iván Fernández[,1], Iván Prieto[***,1], Benito Alén[1], Antonio García-Martín[1], José M. Llorens[1], S. R. J. Brueck[2], and José M. Ripalda[*,1]**

[1] IMM-Instituto de Microelectrónica de Madrid (CNM-CSIC), Isaac Newton 8, PTM, E-28760 Tres Cantos, Madrid, Spain
[2] Center for High Technology Materials, University of New Mexico, Albuquerque, NM 87106, USA

Received 7 October 2015, revised 27 November 2015, accepted 27 November 2015
Published online 4 December 2015

Keywords photovoltaics, plasmonics, metals, nanowires, semiconductors, contacts

* Corresponding author: e-mail j.ripalda@csic.es
** Currently at Nano4Energy SL: http://nano4energy.eu/
*** Currently at ETH Zurich Laboratory for Solid State Physics HPF F2, Otto-Stern Weg 1, 8093 Zürich, Switzerland

We demonstrate high optical transmission in solar cell contacts based on nanowire arrays with subwavelength spacing. The photocurrent results obtained from fabricated devices are compared with numerical simulations. The proposed contact design leads to optical losses significantly smaller than the fraction of the top surface taken up by the metallic contact (<10% vs. 36%). The resulting sheet resistance of the contact is 46.7 Ω/square, comparing favourably with transparent conductive oxides.

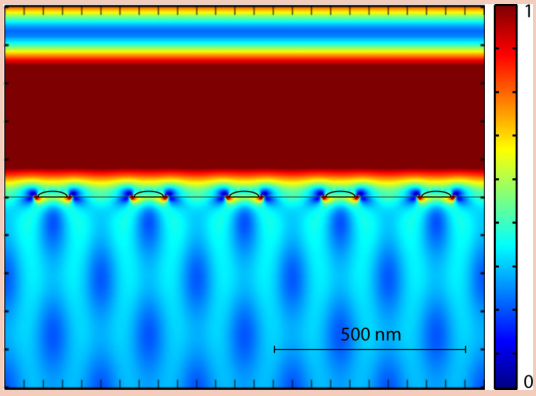

Normalized electric field magnitude at λ = 887 nm, polarization perpendicular to the nanowires. The black contours indicate the position of the nanowires and the GaAs surface. The reflected wave-front is undisturbed by the subwavelength array (period = 250 nm), but the transmitted light is strongly scattered in a Talbot effect pattern.

1 Introduction Electrical current collection at the front side of optoelectronic devices typically requires covering a fraction of the area of the device with metallic conductors, thus sacrificing a fraction of the incoming light. Transparent conductive oxides such as indium tin oxide (ITO) can also be used, but these present a similar compromise between electrical conductivity and optical transparency while having the added problems of indium scarcity and material brittleness [1, 2]. Due to technological constraints, the width of the metallization fingers is typically larger than a few microns [3]. The spacing of the fingers must always be kept large in proportion to finger width in order to minimize optical shadowing losses. Thus, both the finger width and the finger spacing are typically much larger than the light wavelength, and the shadow factor can be directly obtained as the ratio of the geometrical area taken up by the contact metal to the area of the device. If those constraints are overcome, as the finger width is reduced to subwavelength dimensions, ray tracing optics fails to provide an adequate description of the system, and the effective shadow factor can only be obtained through wave optics or experimental measurements [4]. Wang et al. have self-consistently solved the electrical and optical parts of the problem to study light harvesting by subwavelength

structures [5]. An interesting feature of subwavelength particles is their increased scattering cross section which can be used to enhance the optical path length inside the device [6, 7] in a similar fashion to the textured surfaces studied by Yablonovitch [8, 9]. The light trapping effect on solar cells can be particularly high when metallic nanoparticles are used due to the excitation of surface plasmon resonances [10, 11], reducing reflection losses and enhancing the optical path length inside the device [12]. It is thus an interesting possibility to use metallic nanostructures as contacts for solar cells. Previous works on the design of plasmonic solar cells are typically based on randomly distributed nanoparticles on the front surface [13, 14] and also on gridlike back contacts [15], but fewer studies are found on the nanostructuration of the necessary front contact grid [16–20]. To maintain the electrical performance as the finger width is reduced, the line spacing must be also reduced in proportion. Eventually a second important threshold is reached: the array period becomes smaller than the free space wavelength of the incoming light. This eliminates back diffraction into air, except for 0^{th} order reflection, and thus increases the coupling of light to the solar cell [21–24]. The influence of similar photonic effects on the Shockley-Queisser limit has been studied analytically by Munday [25, 26]. Experimentally, the transmission of metal nanowires has been mostly studied optically on bare substrates [27, 28], or through photocurrent measurements on devices based on low refractive index materials [29]. Here we present results obtained in devices fabricated with inorganic semiconductors whose high refractive index significantly alters light coupling. We use simulations and experimental measurements on fabricated devices to study a case where not only the finger width is in the subwavelength regime, but the finger spacing is as well. We find that the resulting shadow factor is much lower than that expected from ray tracing, opening new opportunities for device engineering. Although we have studied the case of photodetectors, the results can also be applied to light emitting diodes and other optoelectronic devices [13].

2 Methods To demonstrate the effect of reduced shadowing, we have fabricated GaAs p/n photodetector devices covered with arrays of 90 nm wide gold wires and compared experimental measurements with simulations of effective shadow factor as a function of wavelength and polarization. A large geometric shadow factor (36%, 250 nm period) has been chosen to make any effect beyond ray tracing optics clearly detectable. The epitaxy is a GaAs p on n structure with the junction 50 nm below the surface without minority carrier confinement layers. A central 300 µm diameter circular window was opened for the entrance of light and a bus frame for current extraction was defined by photolithography and e-beam evaporation of Ti/Pt/Au (5/10/50 nm). The grids were fabricated by electron beam lithography (EBL) at 25 kV and 16 pA on 250 nm thick PMMA resist. An interferometric sample stage was used to cover the whole device area (300 µm diameter) with 25 × 25 μm^2 e-beam exposure fields. Metal patterns were defined by Mo/Au (5/15 nm) magnetron sputtering and PMMA resist lift-off. The 5 nm Mo layer was necessary to improve adhesion. The photocurrent generated by light modulated at 477 Hz was collected through 20 µm diameter tungsten probes and demodulated using a lock-in amplifier at low photon flux to minimize the possible effect of a higher series resistance of the reference devices (without nanowires). The light from a halogen lamp was dispersed by a 0.3 m focal length monochromator set to a spectral resolution of ~1 nm and then coupled into a 200 µm core size multimode optical fiber. Light coming out from the fiber was collimated again and linearly polarized parallel or perpendicular to the grid direction using a fixed Glan–Thompson polarizer and a rotating achromatic half wave retarder. The polarized beam was then focused onto the device within a 300 µm diameter spot using a low magnification objective lens (NA = 0.15). We report the experimental shadow factor as:

$$S = (P_0 - P_N)/P_0 \,, \tag{1}$$

where P_N and P_0 are the experimentally measured photocurrents for the nanowire and reference devices, respectively.

The FDTD Solutions, Lumerical Inc., software was used to simulate light reflection and absorption [30]. The obtained absorption profile as a function of depth into the device was used as input for numerically solving the fully coupled non-linear equations for electron and hole transport using the PC1D code by Basore [31]. In this case it is a good approximation to reduce the transport equations to one dimension because the device periodicity is an order of magnitude smaller than the diffusion lengths in GaAs (typically ranging from 2 to 10 µm) [32]. The simulated shadow factors S_S have been calculated by substituting the photocurrents in Eq. (1) with the product of the light flux entering the semiconductor surface T, times the internal quantum efficiency Q obtained from solving the transport equations:

$$S_S = (Q_0T_0 - Q_NT_N)/(Q_0T_0) \,, \tag{2}$$

where the N and 0 subscripts correspond to the nanowire and reference devices, respectively. The fractions of the losses attributable to reflection S_R and metal absorption S_A are obtained as

$$S_R = (Q_NR_N - Q_0R_0)/(Q_0T_0) \,, \tag{3}$$

$$S_A = (Q_NA_N - Q_0A_0)/(Q_0T_0) \,, \tag{4}$$

where R_N and R_0 are the fluxes at the reflection monitors and absorption is given by $A = 1 - R - T$. Due to the fact that the shadow factor as defined in Eq. (2) is not purely optical, S_S only equals $S_R + S_A$ if $Q_N = Q_0$.

3 Results and discussion The experimental results are compared in Fig. 1 with the FDTD simulations. The

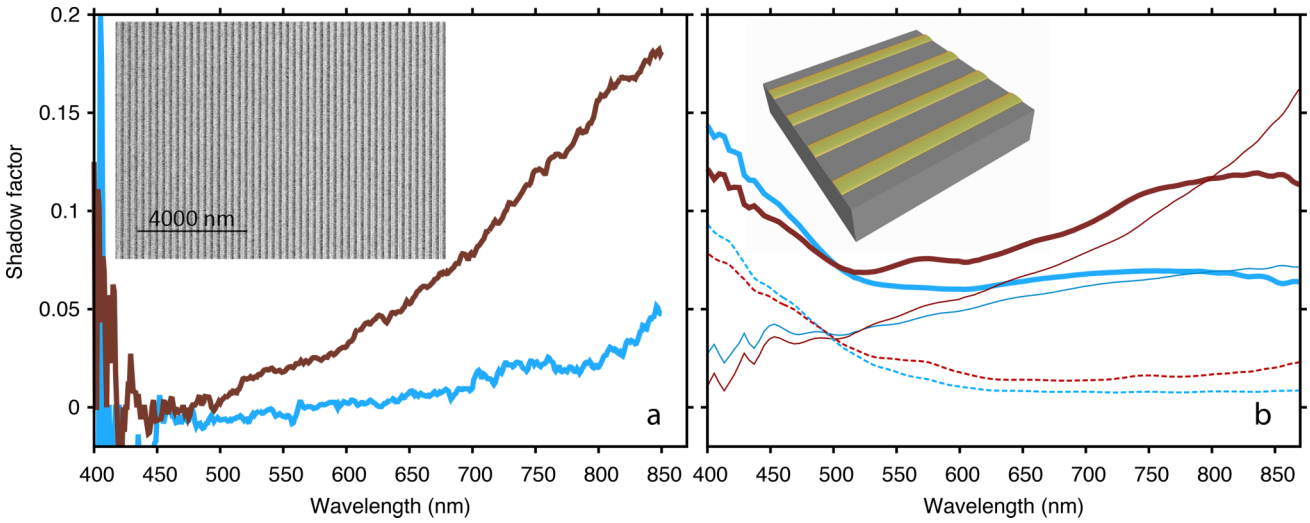

Figure 1 Experimental and simulated shadow factors for gold nanowires on a GaAs photodetector. Dark red and light blue represent results for polarization transversal and parallel to the nanowires, respectively. (a) Experimental shadow factors resulting from comparing the photocurrent with and without gold nanowires on GaAs photodetector devices. The inset shows a scanning electron microscope image of the gold wire array. (b) Simulations of the photocurrent loss caused by the nanowire shadow. The thick lines represent the simulated S_S shadow factor as defined in Eq. (2). The thin solid lines represent the losses caused only by reflection in the nanowires, S_R as defined in Eq. (3). The dashed lines represent the losses caused only by absorption in the nanowires, S_A as defined in Eq. (4). Electronic transport effects offset some of the optical losses at long wavelengths.

reduction of the shadow factor is remarkable as compared with the geometrical estimate of 36%. The nanowire array makes the devices very sensitive to the polarization of incoming light due to the coupling of transverse polarized light to localized surface plasmons. Experimentally the reference and nanowire devices yield almost the same photocurrent at high photon energy, making the apparent shadow factor nearly zero. Among several concurrent effects such as waveguide cut-off filtering [8], or localized plasmonic resonances, an important cause for the reduced shadowing in our experiments is the fact that the period of the nanostructure is such that only the 0^{th} diffraction order is reflected back into air, whereas several diffraction orders exist within the solar cell due to the higher refractive index of the semiconductor. According to our calculations, the increased shadowing at longer wavelengths for transversal polarized light is due to a broad localized surface plasmon resonance centered at 1070 nm. This resonance can be shifted towards longer wavelengths by increasing the perimeter of the nanowire cross section [4], suggesting that there still is ample room for further optimization of these nanowire arrays. The simulated S_S shadow factor (thick lines in Fig. 1b) is higher at the shortest wavelengths than the measured result, but has good qualitative agreement with experiment at longer wavelengths and reproduces the effect of light polarization observed experimentally. Most importantly, both experiment and simulation demonstrate shadowing losses lower than those corresponding to the geometric area of the contacts.

To eliminate the need to compare results from different devices, we have also measured the photocurrent generated by a 30 µm diameter spot using direct tungsten halogen illumination, and obtained the shadow factor by comparing the photocurrent obtained in areas with and without nanowires in the same device. By this procedure, averaging both polarizations in a broadband wavelength range (only limited by device responsivity), we obtain a shadow factor of 4%, much smaller than the 36% geometrical shadow factor in our nanowire array, and in good agreement with the experimental data in Fig. 1. The measured sheet resistance of our nanowire grid is 46.7 Ω/square. For comparison, a 110 nm thick ITO layer has a sheet resistance of 63.6 Ω/square, and a transmission of 93% [29].

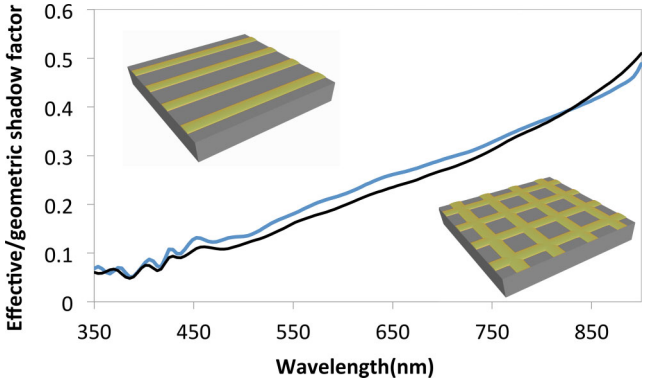

Figure 2 Results for 1D wire arrays carry over to 2D. Simulated polarization averaged shadowing efficiency (S_R) for a 1D wire array (blue line) and a 2D square grid (black line) with the same period (250 nm), wire dimensions (90 nm wide, 15 nm thick) and composition (Au/GaAs). For simplicity, in these simulations all internal quantum efficiencies are set to 1.

4 Extension to the 2D case We have studied 1D arrays to discern polarization effects, but our results readily translate to 2D nanowire arrays in a mesh pattern, as can be seen in the simulation results of Fig. 2. This conclusion is also supported by the results reported by Catrysse et al. [16]. Minor differences between the 1D and 2D cases can be attributed to the excitation of delocalized, propagating surface plasmon polaritons (SPP) in the 2D case [19], SPPs propagating along the wire length can not be excited in the 1D case because the reciprocal lattice vectors of the wire array are perpendicular to the wires, and thus these cannot provide the required momentum matching. In the 2D case, diffraction causes light-SPP coupling through the reciprocal lattice vectors of the 2D array.

5 Conclusion We demonstrate nanowire arrays with subwavelength periodicity as a promising alternative to transparent conductive oxides. Both experiment and simulations demonstrate optical losses that represent a small fraction of the area taken up by the metal contact. Results are presented as a function of light polarization for a 1D array, but readily translate to 2D arrays and unpolarized light by averaging the results obtained for both polarizations.

Acknowledgements We acknowledge the financial support of MINECO (ENE2012-37804-C02-02 and AIC-B-2011-0806) and Community of Madrid (S2013/MAE-2780).

References

[1] C. C. Wu, C. I. Wu, J. C. Sturm, and A. Kahn, Appl. Phys. Lett. **70**, 1348 (1997).
[2] M. Cai et al., Adv. Mater. **24**, 4337 (2012).
[3] I. García, I. Rey-Stolle, B. Galiana, and C. A. Algora Appl. Phys. Lett. **94**, 053509 (2009).
[4] C. F. Bohren and D. R. Huffman, Absorption and Scattering of Light by Small Particles (Wiley, 2008).
[5] X. Wang, M. R. Khan, M. Lundstrom, and P. Bermel, Opt. Express **22**, A344 (2014).
[6] D. M. Callahan, J. N. Munday, and H. Atwater, Nano Lett. **12**, 214 (2012).
[7] S. Mokkapati and K. R. Catchpole, J. Appl. Phys. **112**, 101101 (2012).
[8] E. Yablonovitch and G. D. Cody, IEEE Trans. Electron Devices **29**, 300 (1982).
[9] V. Ganapati, O. D. Miller, and E. Yablonovitch, IEEE J. Photovolt. **4**, 175 (2014).
[10] H. A. Atwater and A. Polman, Nature Mater. **9**, 205 (2010).
[11] S. Pillai and M. A. Green, Sol. Energy Mater. Sol. Cells PVSEC **18**, 94, 1481 (2010).
[12] N. P. Hylton et al., Sci. Rep. **3**, 2874 (2013).
[13] K. R. Catchpole and A. Polman, Appl. Phys. Lett. **93**, 191113 (2008).
[14] V. E. Ferry, J. N. Munday, and H. A. Atwater, Adv. Mater. **22**, 4794 (2010).
[15] V. E. Ferry, L. A. Sweatlock, D. Pacifici, and H. A. Atwater, Nano Lett. **8**, 4391 (2008).
[16] P. B. Catrysse and S. Fan, Nano Lett. **10**, 2944 (2010).
[17] J. N. Munday and H. A. Atwater, Nano Lett. **11**, 2195 (2011).
[18] K. Aydin, V. E. Ferry, R. M. Briggs, and H. A. Atwater, Nature Commun. **2**, 517 (2011).
[19] J. Van de Groep, P. Spinelli, and A. Polman, Nano Lett. **12**, 3138 (2012).
[20] D. Sammito, P. Zilio, G. Zacco, J. Janusonis, and F. Romanato, Nano Energy **2**, 337 (2013).
[21] Z. Yu, A. Aaswath, and S. Fan, Proc. Ntl. Acad. Sci. **107**, 17491 (2010).
[22] S. Mokkapati and K. R. Catchpole, J. Appl. Phys. **112**, 101101 (2012).
[23] J. Buencuerpo, J. M. Llorens, M. L. Dotor, and J. M. Ripalda, Appl. Phys. Lett. **103**, 083901 (2013).
[24] J. Buencuerpo, J. M. Llorens, M. L. Dotor, and J. M. Ripalda, Opt. Express **23**, A233 (2015).
[25] J. N. Munday, J. Appl. Phys. **112**, 064501 (2012).
[26] Y. Xu and J. N. Munday, IEEE J. Photovolt. **4**, 233 (2014).
[27] H. Wu et al., Nature Nanotechnol. **8**, 421 (2013).
[28] I. Massiot, N. Vandamme, N. Bardou, C. Dupuis, A. Lemaitre, J. F. Guillemoles, and S. Collin, ACS Photon. **1**, 878 (2014).
[29] J. Van de Groep et al., Sci. Rep. **5**, 11414 (2015).
[30] The 5 nm thick Mo adhesion layer is expected to be in the form of a complex suboxide mixed with the GaAs native oxide due to the very reactive nature of Mo atoms impacting the substrate during sputtering deposition. The optical properties of such a complex and thin layer are difficult to ascertain, thus it has not been included in our simulations.
[31] P. A. Basore, IEEE Trans. Electron Devices **37**, 337 (1990).
[32] S. Adachi, Properties of Group IV, III–V and II–VI Semiconductors (Wiley, Chichester, 2005).